

Henry Ford Health

## Henry Ford Health Scholarly Commons

---

Neurology Articles

Neurology

---

8-26-2022

### Application of Neuromelanin MR Imaging in Parkinson Disease

Naying He

Yongsheng Chen

Peter A. LeWitt

*Henry Ford Health*, PLEWITT1@hfhs.org

Fuhua Yan

E. Mark Haacke

Follow this and additional works at: [https://scholarlycommons.henryford.com/neurology\\_articles](https://scholarlycommons.henryford.com/neurology_articles)



---

#### Recommended Citation

He N, Chen Y, LeWitt PA, Yan F, and Haacke EM. Application of Neuromelanin MR Imaging in Parkinson Disease. *J Magn Reson Imaging* 2022.

This Article is brought to you for free and open access by the Neurology at Henry Ford Health Scholarly Commons. It has been accepted for inclusion in Neurology Articles by an authorized administrator of Henry Ford Health Scholarly Commons.

# Application of Neuromelanin MR Imaging in Parkinson Disease

Naying He, MD, PhD,<sup>1</sup> Yongsheng Chen, PhD,<sup>2</sup>  Peter A. LeWitt, MD,<sup>2,3</sup>  
Fuhua Yan, MD, PhD,<sup>1\*</sup>  and E. Mark Haacke, PhD<sup>1,2,4,5</sup>

MRI has been used to develop biomarkers for movement disorders such as Parkinson disease (PD) and other neurodegenerative disorders with parkinsonism such as progressive supranuclear palsy and multiple system atrophy. One of these imaging biomarkers is neuromelanin (NM), whose integrity can be assessed from its contrast and volume. NM is found mainly in certain brain stem structures, namely, the substantia nigra pars compacta (SNpc), the ventral tegmental area, and the locus coeruleus. Another major biomarker is brain iron, which often increases in concert with NM degeneration. These biomarkers have the potential to improve diagnostic certainty in differentiating between PD and other neurodegenerative disorders similar to PD, as well as provide a better understanding of pathophysiology. Mapping NM *in vivo* has clinical importance for gauging the premotor phase of PD when there is a greater than 50% loss of dopaminergic SNpc melanized neurons. As a metal ion chelator, NM can absorb iron. When NM is released from neurons, it deposits iron into the intracellular tissues of the SNpc; the result is iron that can be imaged and measured using quantitative susceptibility mapping. An increase of iron also leads to the disappearance of the nigrosome-1 sign, another neuroimage biomarker for PD. Therefore, mapping NM and iron changes in the SNpc are a practical means for improving early diagnosis of PD and in monitoring disease progression. In this review, we discuss the functions and location of NM, how NM-MRI is performed, the automatic mapping of NM and iron content, how NM-related imaging biomarkers can be used to enhance PD diagnosis and differentiate it from other neurodegenerative disorders, and potential advances in NM imaging methods. With major advances currently evolving for rapid imaging and artificial intelligence, NM-related biomarkers are likely to have increasingly important roles for enhancing diagnostic capabilities in PD.

**Evidence Level:** 1

**Technical Efficacy:** Stage 2

J. MAGN. RESON. IMAGING 2022.

**M**RI offers a variety of imaging methods to produce quantitative measurements and spatial information about the human brain. Specifically, it can be used to provide exquisite structural imaging via high-resolution T<sub>1</sub>-weighted (T<sub>1</sub>W) images, measurement of iron content through quantitative susceptibility mapping (QSM), neuromelanin (NM) mapping through NM-MRI sequences, white matter tractography through diffusion tensor imaging (DTI) and network connections through resting-state functional MRI. For achieving unmet needs of movement disorders research, one of the major

areas of interest today is assessing the presence and integrity of NM (in terms of the contrast and volume) in the brain stem, mostly located in the substantia nigra pars compacta (SNpc), ventral tegmental area (VTA), and locus coeruleus (LC). Another area of increasing interest is mapping the iron content in deep grey matter (DGM) structures. These two biomarkers go hand in hand as will be seen as the background for NM imaging unfolds.

Since available treatments for PD are still only for symptomatic relief and fail to stop the neurodegeneration progress,

View this article online at [wileyonlinelibrary.com](https://onlinelibrary.wiley.com/doi/10.1002/jmri.28414). DOI: 10.1002/jmri.28414

Received May 22, 2022, Accepted for publication Aug 3, 2022.

\*Address reprint requests to: F.Y., Department of Radiology, Ruijin Hospital, Shanghai Jiao Tong University School of Medicine, No. 197 Ruijin Er Road, Shanghai 200025, China. E-mail: [yfh11655@rjh.com.cn](mailto:yfh11655@rjh.com.cn)

From the <sup>1</sup>Department of Radiology, Ruijin Hospital, Shanghai Jiao Tong University School of Medicine, China; <sup>2</sup>Department of Neurology, Wayne State University School of Medicine, Detroit, Michigan, USA; <sup>3</sup>Department of Neurology, Henry Ford Hospital, Parkinson's Disease and Movement Disorders Program, Detroit, Michigan, USA; <sup>4</sup>Department of Radiology, Wayne State University School of Medicine, Detroit, Michigan, USA; and <sup>5</sup>SpinTech, Inc, Bingham Farms, Michigan, USA

Additional supporting information may be found in the online version of this article

This is an open access article under the terms of the [Creative Commons Attribution-NonCommercial-NoDerivs](https://creativecommons.org/licenses/by-nc-nd/4.0/) License, which permits use and distribution in any medium, provided the original work is properly cited, the use is non-commercial and no modifications or adaptations are made.

early-stage PD biomarkers are sought to better understand the pathophysiology, improve detection, and enable the application of timely clinical interventions. Furthermore, sensitive biomarkers of disease progression may speed up the process of developing disease modification therapies. The reason mapping NM is so important is that before PD motor symptoms emerge, there is already a greater than 50% loss of dopaminergic melanized neurons in the SNpc.<sup>1</sup> The earliest and greatest loss occurs in the nigrosome-1 (N1) territory, which is located in the caudal and mediolateral portions of the SNpc.<sup>2</sup> As a metal chelator, NM is thought to absorb iron, thereby protecting the dopaminergic neuron. If the NM can no longer function as an iron chelator (whether it is already fully saturated with iron and, hence, unable to absorb more of these ions, or for another reason), there may be release of previously intracellular iron in adjacent tissue.<sup>3</sup> Usually, neuronal death occurs at this stage since the NM can no longer protect the dopaminergic neurons. This deposited iron is in the form of ferritin and, therefore, becomes visible by MRI. Evidence shows that, concurrent with this loss, there is an increase of iron deposition in the SNpc in the PD brain.<sup>3</sup> Therefore, imaging NM and iron changes in the SNpc have proven to be valuable in facilitating the early diagnosis of PD and in monitoring disease progression.

During this process, it also appears that, in the PD brain, the NM-containing structures (SNpc and LC) and the entire SN (SNpc plus substantia nigra pars reticulata [SNpr]) undergo significant atrophy.<sup>4–6</sup> Loss of the NM manifests as a loss of the N1 sign<sup>7</sup> and an increase of iron content.<sup>4,8,9</sup> In PD patients, in the N1 territory where the earliest and greatest loss of NM occurs,<sup>2</sup> an increase in iron deposition is also found.<sup>10</sup> Recent studies have demonstrated NM loss and an increase in iron in the SNpc as valuable imaging biomarkers in PD.<sup>11</sup> We have found that these imaging measures (NM volume in the SN, N1 visualization, iron content in the entire SN, and the SN volume), when combined, provide a promising diagnostic biomarker for early-stage PD patients.<sup>4</sup> Furthermore, neuronal loss in the ascending noradrenergic projections from the LC occurs in PD.<sup>12</sup> Degeneration of NM-containing LC neurons precedes the loss of NM-containing SN neurons in PD brain and may represent some of the earliest evidence for the development of PD.<sup>12</sup> Therefore, the need to enhance the tools for imaging the LC has become increasingly important.<sup>13</sup>

The current approach of NM-MRI is to use magnetization transfer contrast (MTC) radiofrequency (RF) pulses to suppress the surrounding macromolecule-rich white matter with little effect on tissue with high-water content such as the NM in the SN and LC.<sup>14</sup> These RF pulses have high specific absorption rates (which require a long repetition time) so that practical approaches to scanning are often carried out to measure only a small section of the brain.<sup>4</sup> Furthermore, imaging the NM in the SN and LC using a three-dimensional (3D) gradient echo

method requires multiple scans in which optimal parameters are imposed separately for the two territories.<sup>13</sup> The iron content of the SN is measured using QSM, which has become a well-established method. QSM is typically processed from susceptibility-weighted imaging (SWI) phase data and it is also used to assess N1 sign visualization. A recent study demonstrated the feasibility of simultaneously imaging NM volume and iron content in PD patients.<sup>4</sup>

The aim of this review is to discuss the following: 1) the function, location, and degeneration of NM in PD; 2) how it is visualized in cadaver brains and in MRI *in vivo*; 3) how NM-MRI is performed and why it works; 4) the evidence showing that NM-MRI correlates with other measures of NM; 5) new approaches to mapping NM and creating a clinical tool for mapping NM automatically; 6) the ability of imaging biomarkers to distinguish PD patients from healthy controls (HCs) and differentiate PD from other movement disorder patients; and 7) future directions of NM-MRI in imaging PD.

We performed a literature search on PubMed and Google Scholar using multiple combinations of keywords including “MRI,” “magnetic resonance imaging,” “neuromelanin,” “NM,” “NM-MRI,” “magnetization transfer,” “MTC,” and “Parkinson’s disease”. Only publications written in English with full-text available (through open access and institutional library subscription) were reviewed. In addition, relevant publications identified from the bibliography of review articles, our reading of many papers in the field and other papers based on the best of our knowledge were also included in this comprehensive narrative review. The literature search was initially performed by N.H., Y.C., and E.M. H and subsequently reviewed by the other authors.

## Neuromelanin, Iron, and the N1 Sign in PD

### Neuromelanin and its Relationship With Iron Deposition

NM is an intraneuronal pigment, whose clumped granules are found exclusively in the brain. It is formed from catecholamines acted upon by a process of auto-oxidation. It involves the incorporation of melanin into lipofuscin derived from lysosomes.<sup>15</sup> NM has a brown-black appearance that is evident in an unmagnified inspection of brain tissue. While the process of regional generation of NM is not fully understood, it is known to play several roles in dopaminergic neurons.<sup>16</sup> Studies by Jan Purkinje first recognized NM in 1837.<sup>17</sup> The melanin leading to the creation of NM is a by-product of dopamine synthesis. In SN and LC neurons, the overall content of NM increases with age. Thereafter, a decline in mean NM content has been found, probably due to the continuing loss of the most heavily pigmented neurons with increasing age.<sup>16</sup> In PD, which leads to a much accelerated loss of pigmented neurons compared to the normal aging process, measurements show an 80% reduction in neuronal count relative to healthy controls which was associated

with a 15% reduction of tissue NM content.<sup>18</sup> When neurons die, their NM content can remain in the extra-neuronal tissue or can be taken up in the cytoplasm of macrophages.

There is considerable evidence to link NM formation with exposure to oxidative free radicals. This evidence has also been one of the leading themes of research into the pathogenesis of PD, for which there is also evidence of oxidative stress and telling by-products of this process such as peroxidized lipid structures and transformed molecules like 8-hydroxy-7,8-hydro-2'-deoxyguanosine. In brain regions where NM is abundant—the SN, LC, and dorsal motor nucleus of the vagus nerve—the most prominent loss of neurons is found in PD along with its characteristic tissue finding, the formation of Lewy bodies. One hypothesis for the abundant presence of NM in catecholamine synthesizing is that auto-oxidation of catechol structures to quinones creates NM as a by-product that is difficult for neurons to remove. NM accumulation may be physically disruptive to the health of such neurons since it damages them by inducing mitochondrial-mediated apoptosis. However, this is not necessarily the entire story in PD, since nonpigmented neurons (such as those in the nucleus basalis of Meynert) also undergo prominent loss in PD.<sup>15</sup> The dorsal tier of the SN (which has the greatest content of NM in the SNpc), is a region that undergoes the earliest neuronal loss in PD.<sup>1</sup> However, the ventral tier of the SNpc demonstrates the most neuronal loss as a feature of PD progression.<sup>19</sup>

NM reduces ferric to ferrous iron and stores this iron as an oxyhydroxide (similar to how this occurs in ferritin). NM present in the SNpc/LC can have iron concentrations in the range of 150–300/0–50 µg iron/gm tissue wet weight as it accumulates from 20 years to 80 years of age<sup>20</sup> (and which appears to be predominantly in the form of H-ferritin). The NM in the LC has about 10 times less iron relative to the SNpc.<sup>20</sup> The concentration of NM in the SNpc/LC ranges from 500–4000/1000–3000 µg/g tissue wet weight over the same age range.<sup>20</sup> Given the concentrations of NM in the SNpc/LC and the iron concentrations in NM, one would expect the susceptibility of NM in vivo to be on the order of that in grey matter (50 ppb or roughly 50 µg iron/gm tissue).<sup>21</sup> In the human SN, it has been estimated that the amount of iron present as a NM-Fe complex is 10%–20% of the total iron concentration present in the SN structure.<sup>22</sup>

Therefore, a loss of chelating function and a subsequent increase in *magnetically visible* iron could serve as a biomarker for NM dysfunction, particular the kind of change that might occur in a neurodegenerative disease such as PD. Intraneuronal NM can only be released following cell death of neurons and, hence, its measure would serve as a direct biomarker of cell damage. Once NM is in a depigmented state, it is thought to deposit its chelated iron (and likely other bound metals) into adjacent brain tissue. If this iron is in a reduced state, it can participate in the Fenton reaction and promote the generation

of hydroxyl radicals facilitating regional oxidative stress. If the previously intracellular NM is released into the extracellular space, it can induce microglial activation. One outcome is triggering the production of nitric oxide, superoxide, and hydrogen peroxide. As ferritin is soluble, its iron content can be taken up systemically. In contrast, hemosiderin is insoluble and the iron will be stored there indefinitely. Assuming that the bound iron in NM behaves as in ferritin, then the depigmentation of that iron could lead to free iron or at least unprotected oxyhydroxides. The presence of abnormal reactive levels of ferrous iron may then lead to neuroinflammation through a variety of neurodegenerative processes. There are many studies<sup>4,23</sup> showing increased iron content in areas where NM is lost and also many papers using NM-MRI showing loss of total NM volume for PD patients (see Table S1 for details).

The SNpc NM content changes may play an important role as a biomarker for PD. It is thought that between 50% and 70% of the NM in the SNpc has depigmented before the appearance of PD motor symptoms.<sup>1</sup> The loss of dopaminergic neurons is most obvious in the caudal and ventro-lateral regions of the SNpc in PD patients. Imaging biomarkers that allow for study of the etiology of disease have therapeutic implications and diagnostic importance and are a major goal in neurological research today, and MRI offers multiple biomarkers noninvasively at the sub-millimeter level.

### SN Subregions and the Distribution of Neuromelanin

The SN can be subdivided into two major populations of neurons: the SNpc and the SNpr. Although merged into one another, the SNpc and the SNpr differ greatly in their anatomical configuration and their functional connections.<sup>4</sup> Differentiating between the SNpc and SNpr is not easily accomplished with conventional MRI or even from histopathological staining of CNS tissue given that clusters of SNpc dopaminergic neurons are deeply embedded within the SNpr.<sup>24,25</sup> The SNpr is located in the ventral portion of the SN and has abundant iron content. While the SNpc is situated more dorsally, its identification can also take advantage of differentiation from the SNpr by its lower iron content and the presence of NM (found in neurons that secrete dopamine). This differentiation can be demonstrated through NM-MRI. For this, one of the more promising approaches to understanding the SN structure is using Calbindin D28k staining. Calbindin stains the protein in afferent fibers of the SN neuropil matrix (consisting of GABAergic striatonigral fibers). Calbindin staining also shows the same regions associated with the presence of tyrosine hydroxylase. A high-resolution cadaver brain study<sup>26</sup> using Calbindin D28k staining and 7 T high-resolution (0.67 mm isotropic resolution) MRI validated the earlier demonstration of SN findings by Damier.<sup>2,24</sup> However, they found a mismatch between the Perl stained results and what is shown in T2\*W images (i.e., the high iron content did not always match the

T2\*W images). The authors commented that the nigrosome territories are structures with low iron content, which is in concordance with the low susceptibility seen in these regions.

NM is absent at birth and one paper suggests that it increases in concentration until the ninth decade of life.<sup>19</sup> However, Liu et al<sup>27</sup> reported that the increase in tissue NM concentration levels off in the seventh decade in the LC. Damier et al<sup>2,24</sup> showed that 60% of the NM is found within dopaminergic neurons of the nigral matrix (Calbindin positive) while the other 40% of NM is in the dopaminergic neurons associated with N1–N5 territories. Damier and colleagues note that the loss of NM occurs in the following order from greater to lesser N1 > N2 > N4 > N3 > N5. The N1–N4 structures lie predominantly below the rostral exiting of the third cranial nerve. Above this is N5 and some remnant of N4. N1 can cover as much as 5 mm below this origin; that is, for MRI with a slice thickness of 1.34 mm, it could appear in four to five caudal slices, for example. Note that the N1 can be posterior medial and be adjacent to the N3 posterior lateral in the more caudal slices. The N5 is seen predominantly posteriorly in the more rostral slices (Fig. 1). Cell loss occurs throughout the SN, but the greatest extent of cell loss is found in the nigrosome territories.<sup>2,24</sup> Damier and colleagues note that, from 7 to 32 years after onset, the cell loss is from 75% to 95%. Also, about 80% of the NM loss is from the SN and 20% in the SN pars dorsalis and SN pars lateralis. These observations are in line with reports from Gibb and Lees<sup>19</sup> and from others who have seen similar localization as the most vulnerable regions for NM loss.

### Visualizing and Assessing the N1 Sign With the Guidance of NM-MRI

Damier as well as Gibb and Lees note that orientation is important in defining structures in the SN.<sup>2,19,24</sup> That is certainly true from a 3D imaging perspective as well.<sup>7</sup> The different apparent shapes shown in Fig. 2 demonstrate this

problem. The geometry changes of the N1 shape are shown in Fig. 3. Consider the SN as a cylinder making an angle of 45° to the *x-z* axes and 45° to the *x-y* axes as well. Then with a transverse cut through the cylinder the N1 sign will take on a truncated ellipsoidal shape (Fig. 2f), whereas if the imaging plane is perpendicular to the SN the N1 will look like a small circle and if the plane is parallel to the long axis of the SN it will look like a long oval shape (Fig. 2c,g). The situation is further complicated by the fact that the N1 can sometimes abut the edge of the SN and any iron that is there may not be observable (Fig. 2a,b,e). This lower iron content may require a much longer echo time to become visible. Depending on the amount of iron present, the N1 sign can be seen with echo times as low as 17.5 msec but in other cases, and particularly for younger individuals, it may require an echo time of 30 msec. As the orientation of the imaging plane changes, the N1 sign can become more and more elongated until the plane runs along the long axis of the cylindrical-like structure representing the SN shape (Fig. 3f).

Visualizing the N1 sign is generally performed using a T2\*W gradient echo sequence such as SWI. The usual SWI processing uses a mask on the high-pass filtered phase images. This can enhance the presence of veins and iron but has the drawback that the phase is geometry dependent. Using QSM data instead to create a susceptibility mask, this problem can be avoided.<sup>29,30</sup> This method is referred to as true-SWI (tSWI)<sup>29</sup> or susceptibility map-weighted imaging (SMWI).<sup>30</sup> It is important to use the mask based on QSM of the high-pass filtered phase data (denoted as QSM-hpf), otherwise, since NM can also show iron content, the mask might indiscriminately suppress the signal from the N1 territory rendering the N1 sign invisible. One can use QSM, but sometimes these images show iron in the N1 region and when tSWI is created from these data, it can also suppress the signal from the N1 sign hiding it in a sea of dark signal. Using QSM of the high-pass filtered phase images will remove some of the background

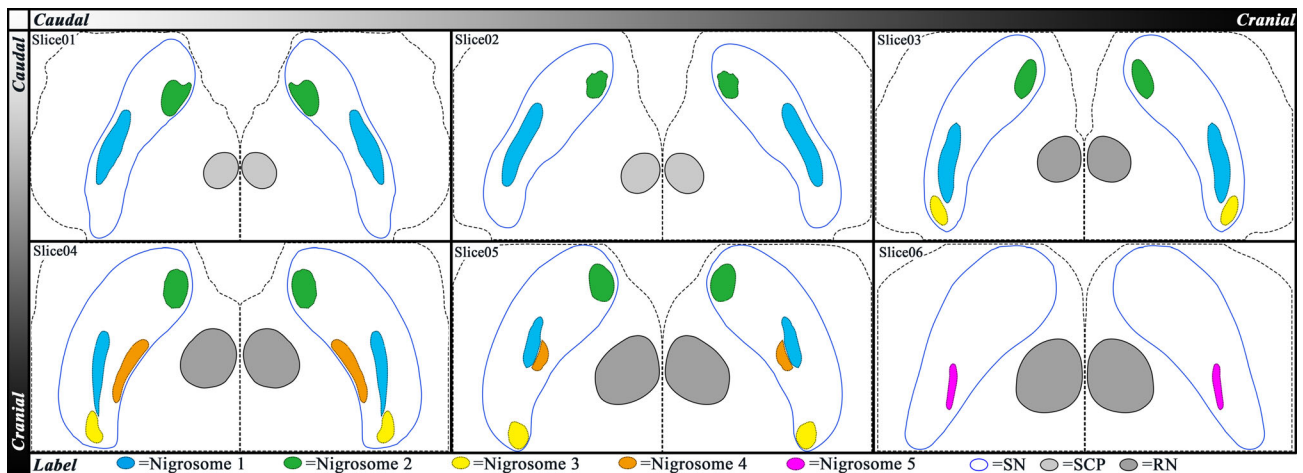


FIGURE 1: The anatomy of the SN and its five nigrosome territories shown on serial axial sections based on figure 1 from the article by Massey et al.<sup>28</sup>



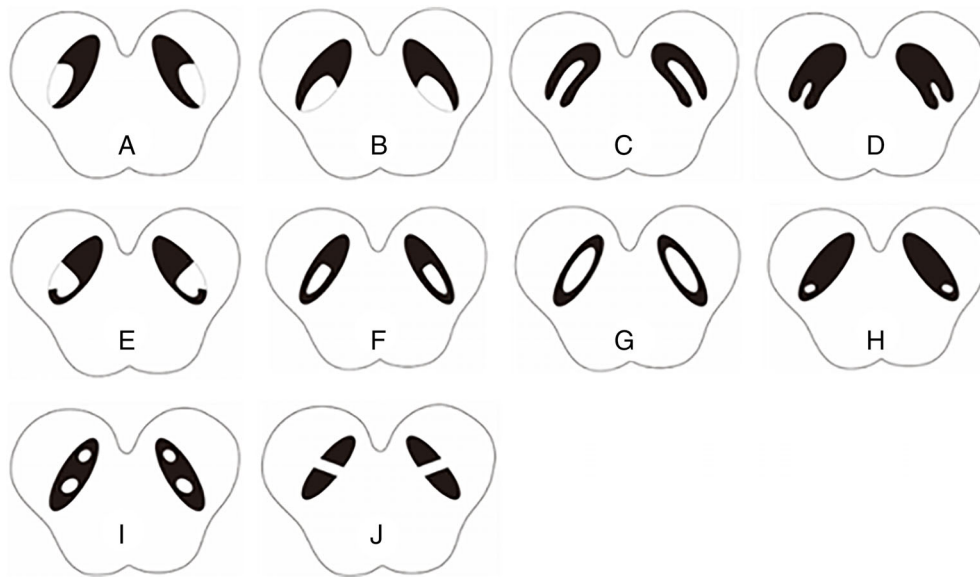


FIGURE 2: Cartoon illustration of the nigrosome 1 variants. Source: Figure reprinted with permission from reference 7 2020 John Wiley & Sons, Inc.

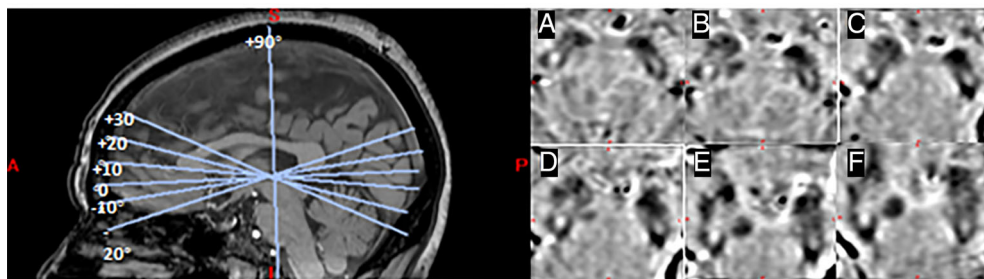


FIGURE 3: (a–f) The N1 sign on QSM-hpf data in a pseudo transverse plane with different degrees of rotation about the y-axis for ( $-20^\circ$ ,  $-10^\circ$ ,  $0^\circ$ ,  $10^\circ$ ,  $20^\circ$ , and  $30^\circ$ , respectively) from a 63-year-old healthy control. The  $0^\circ$  angle represents the original scanning orientation along the anterior commissure–posterior commissure line. The yellow arrows show that as the scanning plane changes from  $-20^\circ$  to  $30^\circ$ , the shape of the N1 becomes more elongated as the angle starts to match the angle to which the SN is tilted away from the transverse plane.

signal and does a better job revealing the N1 sign more consistently. See Fig. 4 for a demonstration of these concepts for a variety of movement disorders including rapid eye movement sleep-behavioral disorder (RBD), postural instability and gait difficulty (PIGD), tremor-dominant (TD), progressive supranuclear palsy (PSP), multiple system atrophy (MSA) with predominant parkinsonism (MSA-P) and cerebellar subtype (MSA-C), essential tremor (ET), and a healthy control (HC) case.

However, interpreting when the N1 sign is present is difficult from its shape alone.<sup>7</sup> Usually when the NM volume is normal and the contrast is high, the N1 sign is clearly present in long echo gradient echo methods like SWI (Fig. 4, HC and ET cases). Likewise, when the NM volume and contrast are low, there will be no N1 sign (Fig. 4, PSP case). We have seen a number of other variants when assessing the N1 sign; even in the presence of NM, there may be no N1 sign; low levels of NM do not guarantee absence of the N1 sign (Fig. 4, RBD and MSA-P) and a small circular bright

structure in the most ventral lateral aspect of the NM territory may represent N3 in the caudal slices. Both T2-weighted spin echo<sup>31</sup> and T2W fluid attenuated inversion recover (FLAIR)<sup>32</sup> sequences have been shown to reveal the N1 sign, but not with as good contrast as that available with long echo gradient echo imaging.<sup>11</sup> In summary, the best way to validate the presence of the N1 sign is to use a variety of images, perhaps the best of which are the overlay of the NM boundaries on the tSWI data.

As a first pass, perhaps the most rapid way to review the data to visualize the N1 sign (or other nigrosome territories) is to have three types of images available: 1) the QSM of the high-pass filter (HPF) data; 2) echo times ranging from 20 msec to 30 msec; and 3) tSWI. Superimposing the boundary of SNpc from the NM-MRI on the SWI or tSWI of QSM of the HPF data will then reveal exactly what structure within the NM that is being visualized. We have noted that NM usually only appears clearly on the short TE NM-MRI data but on occasion it can appear on a longer echo as well.

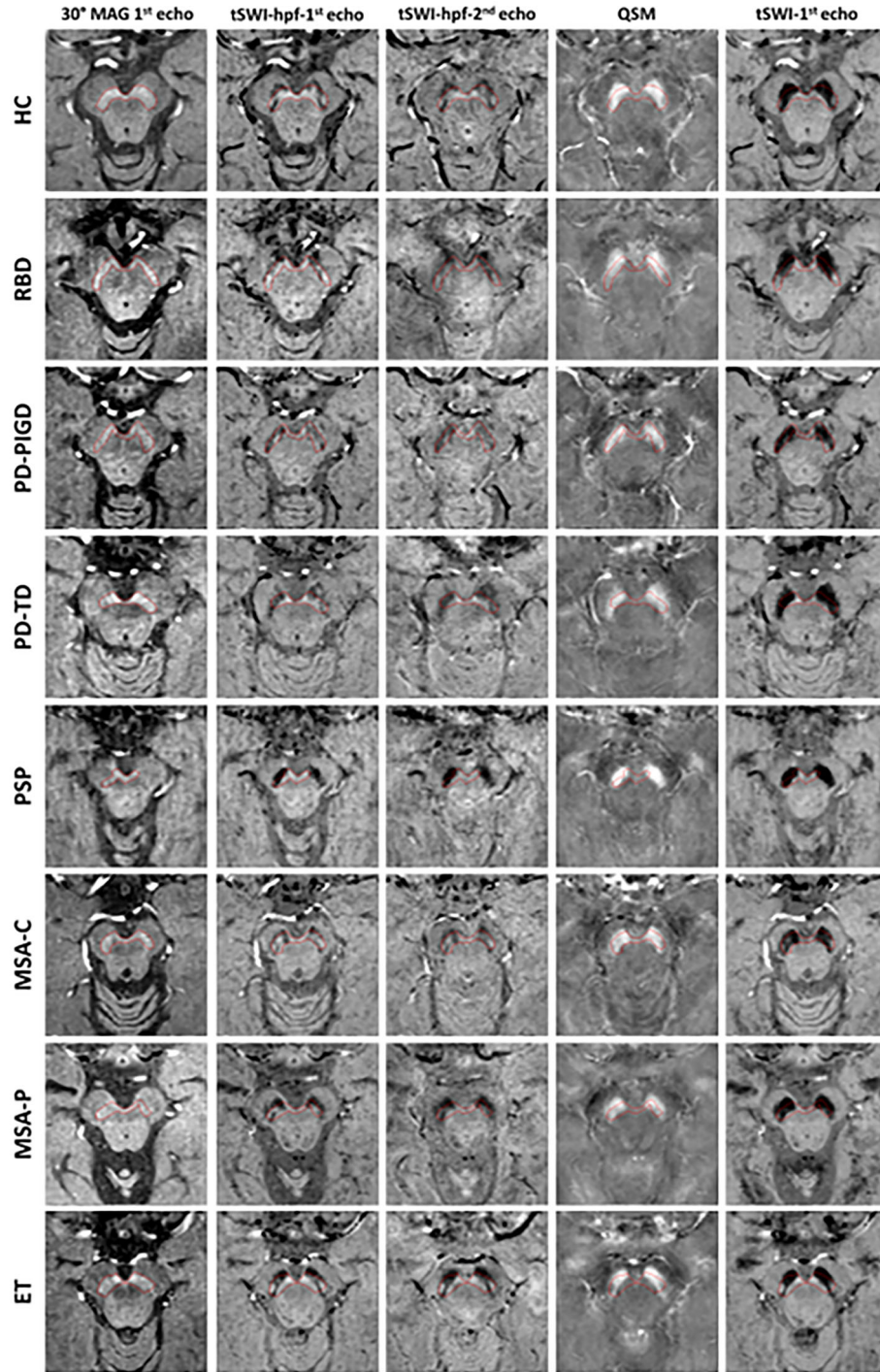


**FIGURE 4:** The presence of the N1 sign in different movement disorders. The five columns represent, in the following order: the original 30° first echo NM image with a resolution of  $0.67 \text{ mm} \times 1 \text{ mm} \times 1.34 \text{ mm}$ ; the tSWI image as applied to the QSM data of the HPF phase from the first echo; the tSWI image as applied to the QSM data of the HPF phase of the third echo; the QSM data over three echoes using MEISWIM; and the tSWI of the first echo using the original QSM data (with no HPF). Since the regions of NM can sometimes have non-zero iron content, using the original QSM can obscure the presence of the N1 sign depending on how the tSWI filter is designed. Hence, we tend to use the tSWI of the QSM data of the HPF phase images for interpreting the presence of the N1 sign. Each row represents a different movement disorder except for the first row, which is for a HC. The ET, RBD, MSA-C, MSA-P and the PD-TD either show bilateral or unilateral N1 signs. The PSP and PI GD cases show bilateral loss of the N1 sign and an atrophied SN. The N4 sign appears to be present in the PI GD case although no N1 sign appears to be present. The red boundaries are from the NM images and are superimposed on all the images to make it clear where the N1 sign must lie if it is to be considered part of the NM territory.

The key take-away point here is that the NM boundaries should be used to validate the interpretation of the N1 sign as first presented by He et al.<sup>4</sup> To appreciate more the

variability of imaging type, Fig. 5 shows the tSWI approach applied to different echoes and several other imaging modalities such as R2\* and QSM maps. The R2\* image shows the

iron regions as bright. The QSM image looks quite different and shows a single medial leg on each SN. The application of tSWI to each of the first five echoes is revealing. Since there is no dephasing in the first echo, it is necessary to see the N1 sign. The advantage is that the NM is still very bright on the first echo and so the contrast between the iron containing regions and NM is enhanced. Note that the NM disappears as the echo times increase (due to the high  $R2^*$  values in these regions).

When there is sufficient signal-to-noise ratio (SNR), the higher resolution imaging methods<sup>26,33</sup> such as 0.67 mm isotropic or 0.8 mm isotropic can potentially reveal the different nigrosomes.<sup>28</sup> The N2–N5 nigrosomes are more poorly visualized than the N1 in healthy controls.<sup>34</sup> Using NM-MRI and tSWI templates, Sung et al<sup>33</sup> showed that the N1 and N2 signs were separately affected in early-stage idiopathic PD patients. Langley et al<sup>35</sup> used high in-plane resolution (0.39 mm  $\times$  0.39 mm) NM-MRI with an  $R2^*$  map to create a voxel-based morphometry representation of the N1 and N2 signs. Increasing the resolution and SNR with the appropriate sequences may indeed help in the future to identify all of the nigrosome signs in a clinically defined imaging protocol.

### LC Structure and the Distribution of NM

There are several recent reviews<sup>36,37</sup> that provide an excellent overview of the role of NM in the LC, particularly the 2019 review by Betts et al<sup>37</sup> discussing noradrenergic dysfunction in

the LC as a biomarker for neurodegeneration. Based on early postmortem studies,<sup>38</sup> each of the human LC nuclei is approximately 14.5 mm long and 2–2.5 mm in diameter (therefore, with a volume of from 45 mm<sup>3</sup> to 71 mm<sup>3</sup>). The paired LC structures are localized 1 mm anterior to the fourth ventricle, 3 mm left and right from the midline, and centered 14–21 mm above the ponto-medullary junction. LC volumes described in more recent NM-MRI studies show inconsistencies with one another and their volumes are much less than reported in the postmortem study (reported to be from 11.4 mm<sup>3</sup> to 30 mm<sup>3</sup> in healthy controls<sup>39–41</sup> and 8.2 mm<sup>3</sup> in a PD cohort<sup>42</sup>). This underestimate may have arisen from the limited number of thick slices in which the LC has been MR-visible.

In studies of LC NM content and LC NM signal intensity across the lifespan, an inverted U-shaped pattern has been reported.<sup>16</sup> This pattern also has been replicated in postmortem tissue studies<sup>16</sup> and NM-MRI studies.<sup>27</sup> The increase and decrease of NM content may reflect increasing pigmented granule content due to continuous noradrenaline production during adulthood and preceding cell death. In PD and other neurodegenerative disorders, there is clearance of previously intracellular NM, also contributing to the down-direction arm of the U-shaped curve after the onset of neurological disease.<sup>16,27</sup> Therefore, studies of LC NM content need to take into account age-related effects when evaluating different clinical populations.<sup>37</sup>

Some published studies<sup>37,43</sup> found a reduction in LC NM contrast in PD patients independent of the analytic

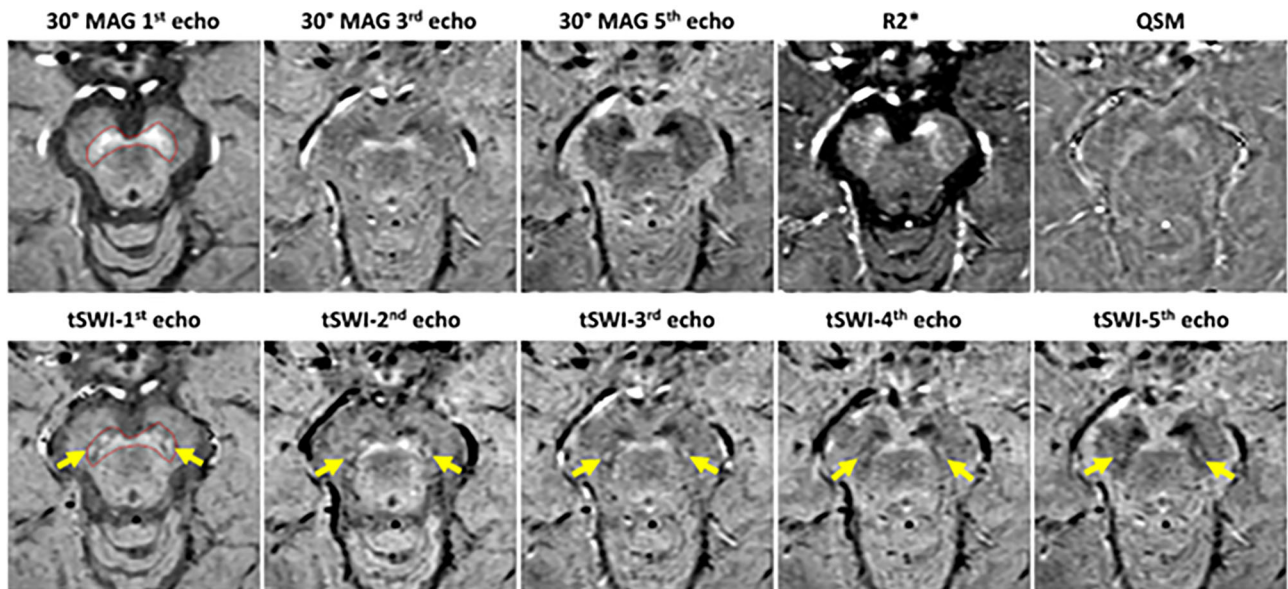


**FIGURE 5:** The role of different image types and different processing. Best visualizing the NM and iron content depend on the MT preparation used, the sequence type used and the choice of imaging parameters. In these data, we used a 3D MT prepared gradient echo SWI sequence with a resolution of 0.67 mm $\times$ 1 mm $\times$ 1.34 mm. These data were collected on a Philips Ingenia scanner. The 30° first echo MTC image in the upper left shows high SNR and visibility. The boundary of the NM is drawn here and copied to the first echo tSWI on the bottom left image. The N1 sign should appear within the NM boundary as is in fact the case. Yellow arrows are then used to highlight the N1 sign in all the lower row tSWI images. This individual has low iron content and so the N1 sign cannot be clearly seen until the fifth echo magnitude image (TE = 37.5 ms). Note the bright region of the N1 is clearly seen even in the early echoes of the tSWI data.



method used (voxel approaches or probabilistic maps). In these studies, the reduction displayed a distinct spatial pattern, with the middle-caudal portion being more affected than the rostral part.<sup>44</sup> However, no significant correlation was observed between LC NM contrast and noradrenaline transporter density in PD patients.<sup>44</sup> A recent study investigated the association of LC structural changes with nonmotor clinical symptomatology in PD and found that there is a spatially heterogeneous degeneration of LC among PD patients. There was an association between regional structural degeneration and individual expressions of PD nonmotor symptoms (such as orthostatic dysregulation or apathy).<sup>43</sup> Another group found a significant positive correlation between LC NM contrast and the extent of motor improvement after levodopa administration.<sup>45</sup> They concluded that evaluating LC NM parameters using NM-MRI might be predictive of levodopa responsiveness in PD.

## Technical Perspectives of NM-MRI

### NM-MRI Sequence Types

NM in the SNpc and LC was first observed by Sasaki and colleagues as hyperintense regions on 2D multislice, high in-plane resolution T1W images acquired with a turbo-spin-echo (TSE) sequence, now referred to as NM-sensitive MRI or NM-MRI.<sup>46</sup> The initial study reported significantly reduced NM contrast in the SNpc and LC regions in PD patients.<sup>46</sup> The contrast in NM-MRI is thought to be associated mainly with the T1-shortening effect when NM is combined with minerals (particularly, iron and copper). What has led to the NM-iron complex being highlighted on T1W images (acquired with TE/TR = 14 msec/600 msec at 3 T) relative to the surrounding white matter or iron-free gray matter is still not clear. The inherent magnetization transfer (MT) effects caused by the high radio-frequency (RF) radiation within a TR and/or a spectral presaturation rf pulse are thought to synergistically contribute to NM image contrast. The 2D TSE sequence employs a high in-plane resolution of less than  $0.5 \times 0.5 \text{ mm}^2$ , with 10 axial slices of 2.5 mm thick slices collected perpendicular to the fourth ventricle. The number of slices were sufficient to cover territory from the rostral slice of the SN caudally to the LC. Other parameters contributing to the NM contrast-to-noise ratio (CNR) include a single concatenation, an echo train length of 2 and avoiding the use of parallel imaging acceleration.<sup>46</sup> Drawbacks of this particular sequence include the high specific absorption rate (SAR) level that would limit the number of slices. Other negative factors include the highly anisotropic voxel size (which impairs the accuracy of the 3D visualization of the SN and LC), volume measurements for the SN and LC, very poor SNR (requiring multiple acquisitions) and very long scan times (>10 minutes), which are prone to motion artifacts when imaging PD patients.

Aiming at achieving shorter scanning times, Nakane and colleagues verified the NM contrast in the SNpc and LC on a 1.5 T scanner using a 3D gradient-recalled-echo (GRE) sequence and an off-resonance MT pulse preparation.<sup>47</sup> The latter study confirmed that the MT effect induced by the off-resonance MT pulse has the most contribution to the observed NM contrast.<sup>47</sup> They also tried to optimize the nominal flip angle of the off-resonance MT pulse for achieving better contrast of the LC and reported that a  $500^\circ$  MT pulse gave improved LC contrast compared to the  $360^\circ$  MT pulse (though it yielded a higher SAR and a longer scan time).<sup>47</sup> Further efforts optimizing the nominal flip angle of the off-resonance MT pulse were carried out by Chen and colleagues.<sup>48</sup> Their study compared the MTC in the SN and LC territories acquired from three sequences: the original 2D TSE sequence, and two 2D GRE sequences with either a nominal  $300^\circ$  MT pulse or a  $300^\circ$  MT pulse applied to the central part of k-space. They concluded that both the GRE sequences were able to mitigate the SAR burden and provide a standardized protocol to image the SN and LC simultaneously. A subsequent study by Trujillo and colleagues employed synthetic melanin-iron complex phantoms at different concentrations to mimic the human SN for a systemic investigation of the contrast mechanisms in NM-MRI.<sup>49</sup> They found that the iron-free melanin phantom produced a negligible MT effect, and the melanin-iron complexes at different concentrations did not alter the observed macromolecular water to free water pool-size-ratio as measured by the quantitative MT method. Instead, the T1 and T2 shortening caused by the melanin-iron complex contributed the most to the observed MT contrast.<sup>49</sup> This report was followed by an in vivo study from the same group,<sup>50</sup> in which they observed a higher water pool-size-ratio of the SNpc in PD patients compared with those in HCs. However, their results need to be considered preliminary given their small sample size. A further study on healthy controls also observed a significantly lower LC water pool-size-ratio compared with surrounding brain tissue.<sup>51</sup> These quantitative MT-derived observations are consistent with studies by Watanabe and colleagues that indicate NM-MRI contrast in the LC is associated with high water content.<sup>52</sup> We have further validated this finding by showing the high contrast of NM using low FAs (in which T1 does not play a significant role<sup>13</sup>) and in mapping actual water content (which also reveals NM<sup>14</sup>).

In line with the needs of 1) quantifying iron deposition in the SN, 2) assessing the N1 sign, and 3) measuring NM contrast and volume in the SNpc and LC to systematically evaluate PD at the early stage, 3D multiecho GRE sequences have received considerable emphasis.<sup>4,13</sup> Liu and colleagues optimized the NM contrast in the SN and LC as a function of flip angles using a multiecho 3D GRE sequence with MT preparation. Their method used an on-resonance 1-2-1 set of binominal RF pulses.<sup>13</sup> The study concluded that the optimal NM contrast in the SN was achieved at a flip angle lower than the Ernst angle of the tissues ( $15^\circ$ – $20^\circ$ ), while the

optimal LC contrast was achieved at a slightly higher flip angle with minor T1 weighting ( $20^{\circ}$ – $25^{\circ}$ ).<sup>13</sup> Meanwhile, the MT prepared multiecho GRE acquisition makes it viable to simultaneously measure the NM content of the SN and the LC from the short echo time-derived MTC images. Iron deposition levels and the N1 evaluation in the SN could be extracted from the SWI and QSM data derived from the long echo times. A subsequent clinical study by He and colleagues<sup>7</sup> used the 3D multiecho GRE method to achieve a better diagnostic performance by combining the NM volume, SN volume, iron content, and the N1 sign in differentiating PD patients from healthy controls. The 3D GRE-based NM-MRI methods benefit from the lower SAR level and larger coverage than is possible with the 2D TSE based methods. Drawbacks of 3D GRE-based NM-MRI methods are mainly associated with susceptibility artifacts and blood flow induced artifacts, which can be mitigated by using a minimum echo time with proper flow compensation.

In summary, the majority of studies<sup>39,53,54</sup> have used the 2D TSE-based sequences for NM-MRI, with or without adding a MT preparation pulse (see Table S2 for imaging parameters). In addition, 2D GRE sequences with MT preparation,<sup>48,55–57</sup> 3D single-echo GRE sequences with MT preparation,<sup>58,59</sup> and 3D multiecho GRE sequences with on-resonance MT preparation<sup>4,13</sup> have also been used for NM-MRI. A direct comparison of 2D TSE sequences with and without MT preparation, and a 3D multiecho GRE sequence is shown in Fig. 6. The detailed imaging parameters of these sequences are listed in Table S2. Briefly, all three scans employed an in-plane resolution of  $0.43 \times 0.86 \text{ mm}^2$ . Sixteen slices with a thickness of 3 mm were acquired in 6 minutes 49 seconds for the 2D TSE sequence without MT preparation, and 9 minutes 36 seconds with MT preparation, which had a longer TR. In contrast, 72 slices with a thickness of 1.5 mm were acquired in 6 minutes 20 seconds for the 3D GRE sequence. The MT pulse is a vendor-provided MT option, which is a 10 msec single lobe sinc pulse with Gaussian apodization,  $500^{\circ}$  nominal flip angle, and 1.2 kHz off-resonance. The three scans shown in Fig. 6 provided comparable NM contrast in the SN and LC. One major advantage of the 3D GRE sequences is that they can provide co-registered SWI and QSM data as well as MRA data comparable with the clinical time-of-flight MRA acquired separately. Overall, with the larger in-plane voxel size, the SNR and CNR in the 3D GRE MT prepared data are higher than those from the limited slice TSE scans. The fast 3D imaging with larger coverage makes it easier to image all DGM structures rapidly, a valuable property for imaging PD patients.

### Imaging Neuromelanin at 7 T

While the vast majority of NM imaging studies in PD patients have been conducted using 3 T MRI scanners, recent developments and applications using 7 T have been

able to show NM contrast in the SN and in the LC using high-resolution imaging.<sup>43,54,60,61</sup> There is no clinical study that directly compares the diagnostic performance of NM loss in the SN using 3 T and 7 T scanners on the same patient population. Independent studies from 3 T<sup>4</sup> and 7 T<sup>61</sup> reported comparable AUC values in differentiating PD patients from healthy controls using the SN volumes measured from the MTC and QSM data. This is not surprising given that the size of the SN and the contrast mechanisms of these data ensure good contrast and reliable measures at 3 T. However, the LC is much smaller than the SN. With increased imaging SNR, 7 T has the potential to provide a much better depiction of the rod-like LC structure.<sup>54</sup> Using 7 T NM-MRI, it is possible to investigate the spatial heterogeneity of LC contrast<sup>43</sup> and regional NM loss in the LC,<sup>60</sup> which are thought to be related to nonmotor symptoms in PD patients.

### NM-Containing Structures, Segmentation, and Template Mapping in the Brainstem

The ability for measurement of NM in the SN or LC and iron in the SN biomarkers to be of practical value will depend on the development of automated processing methods. Today, this option comes in the form of template mapping in which a structure and its boundaries can be defined in template space based on a single high-quality dataset.<sup>25,48,56,62,63</sup> Ideally, data from other individuals of that class (healthy control or patient type) are then mapped to this original dataset and a probability map created from which one can define the extent of the structure. In turn, this template can be mapped to the MNI template and the user can have access to Talairach coordinates. In the early implementations, the atlases created were based on T1 and or T2 data.<sup>56,64</sup> Today, mapping NM and iron in the midbrain use NM and QSM or R2\* data to generate the templates. The boundaries from these templates are then used to map out the SNpc as the overlap between the NM contrast structure and the whole SN. Generally, the template approaches reported so far used NM-MRI for SNpc<sup>56</sup> or QSM data for the SN.<sup>65,66</sup> Recall that hyperintense signal from the MTC N-MMRI sequences is related to the SNpc and VTA.<sup>67</sup>

Most early studies used manual tracing methods. Subsequently, some semi-automated approaches were applied.<sup>48,68</sup> More recently further attempts at full automation have been reported.<sup>25,66</sup> Automated approaches can potentially overcome the limitations of differences between raters and also dramatically reduce the time to process the data. Segmenting the SN and NM can be performed algorithmically or by using artificial intelligence (AI). The former usually involves a clear set of rules while the latter is done ad hoc through a deep learning process, extracting a set of critical features. This process, in practice, could be similar to some of the algorithmic input. Several AI-related papers have been published

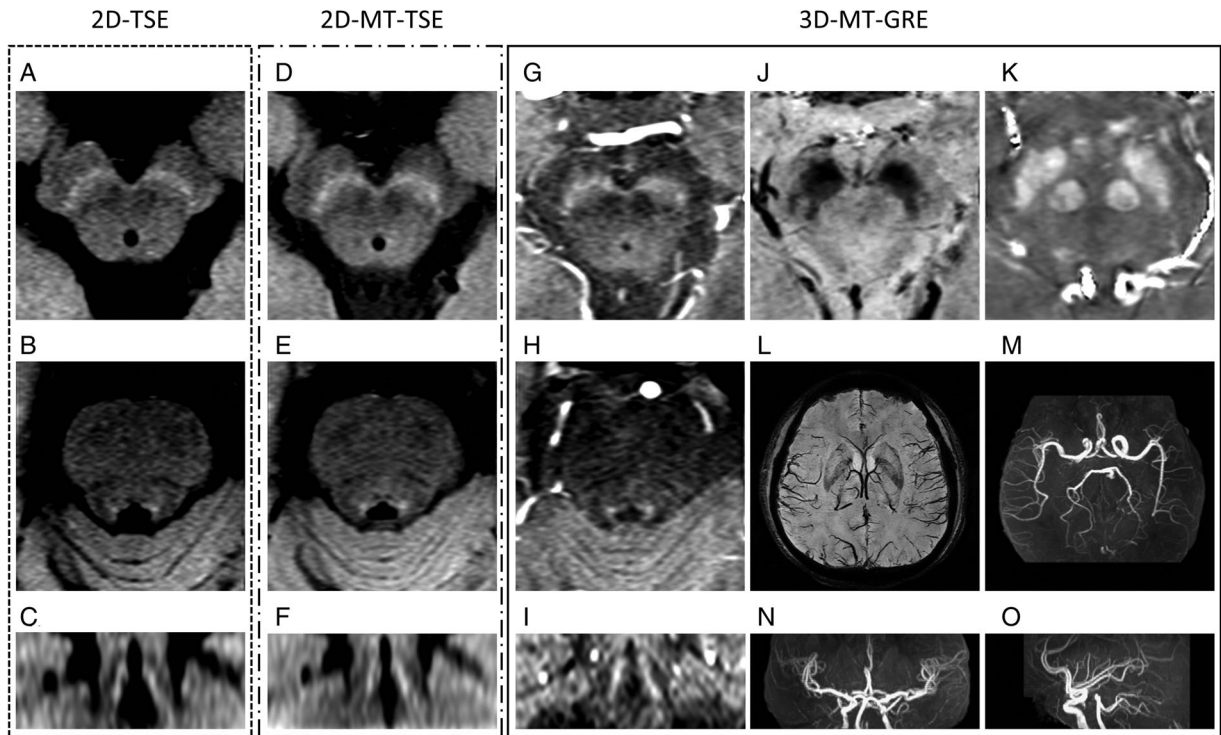


**FIGURE 6:** A direct comparison of 2D TSE and 3D GRE NM-MRI sequences for a 41-year-old man. Images (a)–(c) in the left panel were from the 2D TSE sequence without an MT pulse. Images (d) and (e) in the middle panel were from the 2D TSE sequence with an MT pulse. Images (g)–(o) in the right panel were from the 3D multiecho GRE sequence. All three sequences show the NM reasonably well although the data are still somewhat noisy (a, d, g) and LC (b, e, h) territories. Of note, images (g) and (h) were averaged over two slices to match the slice thickness in the TSE sequences. The reformatted coronal view (c, f, i) showed that the 3D GRE sequence had a sharper depiction of the LC structure given by thin slice 3D acquisition. In addition, the 3D GRE sequence was also used to generate SWI (j and l), QSM (k), and MRA (m–o) images. Data were acquired using a Siemens VERIO 3 T scanner with a 32-channel head coil. Detailed imaging parameters are listed in Table S2.

recently on extracting DGM structures (including the SN).<sup>69,70</sup>

Creating a template from QSM or T2\* data alone cannot separate the SNpc and SNpr because there are no apparent boundaries in these images to differentiate them. However, combined with a template from NM data, the overlap region can be considered to be the SNpc. The remaining region not in the overlap from the NM template can be assumed to be the VTA. Segmenting the VTA has also been of interest in studying fiber pathways with DTI where templates of the VTA have been used, although results have been quite variable.<sup>62,71</sup>

One of the issues with algorithmic methods is setting the contrast threshold above which the structure will be assessed. This can lead to large variations in volumes.<sup>68</sup> AI methods will also depend on the training of the data and their accuracy could be susceptible to how the training is carried out. A recent neural net approach shows much larger than expected NM volumes.<sup>69</sup> Another major issue for comparing data across sites or even over time in the same scanner is normalization. One way to handle this problem is to use a normalized contrast (i.e., the difference between the NM region and an adjacent structure, normalized by the signal of the adjacent structure).<sup>25</sup>

Evaluating the data from a given individual after the template has been created involves mapping that individual's data to the template, picking up the boundaries, mapping them back to the original space, and then fine tuning the boundaries.<sup>25</sup> This approach allows finer details to be found. For example, in some high-resolution data of the NM, fingers can be seen projecting into the crus cerebri. Also fine tuning the boundaries requires high SNR. Therefore, for mapping of the NM in the SN, a slightly lower resolution (which also requires less scan time) will provide much better SNR. For example, reducing the resolution from  $0.44 \times 0.44 \text{ mm}^2$  to  $0.67 \times 0.67 \text{ mm}^2$  will reduce the scan time to 2/3 the original scan time and increase the SNR by a factor of 1.5 to 2 (depending if the higher resolution requires doubling the bandwidth or not). Imaging movement disorder patients is often difficult, so a rapid scan time can be very useful. Also, being able to extract both the NM and iron content from a single scan makes it possible to use each of these variables in clinical assessment and avoids the need for co-registration between different types of scans. One recent approach used a single MTC scan of 5 minutes to accomplish this goal.<sup>4</sup> In the end, mapping the NM may still prove challenging for any

of these methods because the NM varies in shape for some brain diseases and the SN is subject to atrophy.

## NM-MRI Applications in PD and Atypical Parkinsonism

### PD Diagnosis and Clinical Correlation

NM-MRI studies evaluating the diagnostic performance of NM biomarkers' ability to discriminate between HCs and patients with PD were summarized in a recent review.<sup>72</sup> The results showed a pooled sensitivity of 89% (95% confidence interval: 86%–92%) and a pooled specificity of 83% (95% confidence interval: 76%–88%) using NM-MRI to diagnose PD. Using the receiver-operating characteristic (ROC) analysis, the area-under-the-curve (AUC) of the ROC values for the NM complex volume, the total SN volume, the SN iron content, and the N1 sign were 0.960, 0.788, 0.740, and 0.891, respectively.<sup>4</sup> Combining the NM complex volume with the N1 sign led to an AUC value of 0.983.<sup>4</sup> The combination of SN volume, signal intensity, and fractional anisotropy in the NM-sensitive substantia nigra gave a diagnostic accuracy (0.93) for PD.<sup>73</sup>

A longitudinal study found that the total area and contrast ratio of the NM-prominent SN were both negatively correlated with disease duration in PD patients.<sup>6</sup> Unlike that in HCs, the volume of the SNpc progressively reduced for increasing disease severity in PD patients. Furthermore, NM signal changes appeared to start in the posterolateral motor areas of the SN and then progressed to more medial regions.<sup>74</sup> This study also showed that the NM SNR in the bilateral posterolateral SN was significantly negatively correlated with the MDS-UPDRS-III OFF score in the early PD cohort, which is consistent with many other studies.<sup>5,39,75</sup> Therefore, NM-sensitive MRI could be a neuroimaging biomarker to monitor the nigral degeneration and disease progression in PD. Biondetti et al also investigated the concomitant spatial changes in SNpc dopamine-iron, dopamine-NM and NM-iron in PD patients and found that the temporal ordering of dopaminergic changes progressively involved first the sensorimotor, and next the associative and limbic striatal and nigral regions.<sup>10</sup> However, NM volume does not appear to correlate with SN volume loss, suggesting that SN atrophy is on a pathophysiological path different from that which causes NM loss.<sup>4</sup>

In PD patients, the SN NM pathology correlates with motor dysfunction, whereas the NM pathology in the LC is related to cognitive impairment. Therefore, NM measures of the LC could serve as a correlate of another important clinical measure of PD progression, cognitive dysfunction in PD patients.<sup>76</sup> Imaging biomarkers of nonmotor features in PD are a major unmet need for clinical trials research. Investigations of PD brains and incidental Lewy body disease have shown that the intraneuronal-synuclein burden in the LC occurs earlier and can be more severe than the dopaminergic

neuron loss in the same patient's SNpc.<sup>12</sup> Therefore, monitoring the contrast ratio of the LC (LC-CR) and area of the LC may be useful in evaluating the component of PD that is related to cognitive dysfunction. It may also be useful in evaluating mild cognitive impairment.<sup>77</sup> Studies have shown that the LC can be linked to many cognitive functions such as short term and working memory, learning, attention, and sleep architecture (especially rapid eye movement sleep-related behavior).<sup>78</sup> Consequently, changes in the LC NM might correlate with a loss in cognitive abilities with normal ageing or in the context of PD.<sup>79</sup> Complicating the interpretation of these measures are major interindividual differences found with LC visualization and volume determinations observed across populations of healthy subjects.<sup>80</sup> Advanced techniques and multisite, large sample size studies are required to evaluate the reliability in measuring LC degeneration in PD using NM-MRI.<sup>81</sup>

### Differential Diagnosis Between PD and Other Movement Disorders Using NMMRI

Recent advances in multimodal MRI techniques including iron and NM-based sequences allow for a precise characterization of the brain stem damage in PD and contribute to good classification between PD and HCs. However, the more practical challenge clinically is to differentiate PD from other neurodegenerative disorders with Parkinsonism. Among these, the most challenging differentiation scenarios pertain to PSP and the Parkinsonian and cerebellar variants of MSA. Some classic features of regional brain atrophy from routine MRI sequences can enhance diagnostic capabilities in MSA, but these changes occur sometimes years into the development of this disorder.<sup>82</sup> The same can be said regarding PSP.

Previous studies have shown that iron content in the SN predominantly reflects the dopaminergic degeneration and disease progression in PD<sup>83,84</sup> but does not allow for differentiation between PD and MSA patients or between different MSA variants.<sup>85</sup> However, compared with PD, higher iron deposition was found in the putamen in MSA patients,<sup>86</sup> while significantly increased susceptibility values were found in the RN, STN and medial region of the SN in PSP patients.<sup>86</sup> Concerning the differential diagnosis between PD and atypical parkinsonism's using NM-MRI, a previous small sample size study concluded that the contrast ratios of NM in the ventral-lateral SNC was lower in PD ( $n = 30$ ) and MSA-P ( $n = 10$ ) groups than in those with PSP syndrome (PSPS:  $n = 13$ ) and control groups ( $n = 22$ ). The LC contrast ratio was lower in the PD group than in the other groups. The sensitivity and specificity were 60% and 90% for PD vs. MSA-P, 63%–88% and 77%–92% for PD vs. PSPS, and 80% and 85% for MSA-P vs. PSP.<sup>87</sup>

One group showed that significant loss of NM and the N1 sign in the de novo PD group than those in the ET and control groups.<sup>88</sup> Another study reported that ET patients



showed no NM difference in the SN when compared with HCs using NM-MRI.<sup>89</sup> (See, for example, Figure 4 for the ET case.) These findings suggest that NM-MRI may serve as a biomarker to differentiate between PD and ET patients.

As for patients with dementia with Lewy bodies (DLB), the NM intensity of the SN is lower than that in HCs, which is consistent with the autopsy results that NM-containing neurons can be lost in patients with DLB.<sup>90</sup>

### NM-MRI Application in PD Subtypes and Prodromal PD

The clinical symptoms of PD are quite heterogenous and so are the pathological changes underlying different PD subtypes.<sup>91</sup> It has been reported that PIGD patients showed significantly lower NM CNR in the lateral SN compared to TD patients. They found a diagnostic accuracy of 79% (sensitivity 76.5% and specificity 78.6%) in differentiating PIGD from TD patients.<sup>92</sup> This is consistent with another PD subtype group study<sup>93</sup> showing that NM-MRI has a potential diagnostic value to discriminate the clinical PD subtypes (which are important in the study of PD progression and disability).

The NM-MRI measures have also been evaluated in prodromal PD cohorts, which are RBD patients. Sommerauer et al<sup>94</sup> reported that the NM in the LC decreased in patients

with PD patients with RBD as compared to PD patients lacking RBD. This is consistent with another study's findings that found NM intensity reduced more markedly in PD patients with RBD behavior than those lacking it.<sup>78</sup> A subsequent study from the same researchers showed reduced NM signal in the LC/subcoeruleus complex of the patients with RBD but lacking Parkinsonism, suggesting that this complex is affected in the purely RBD subjects to the same degree as it is affected in PD.<sup>95</sup> These results are in agreement with the findings of widespread noradrenergic impairment in RBD, as detected with noradrenaline transporter imaging.<sup>94</sup> These studies also support the potential of NM MRI as an early marker of PD in the prodromal phase (which often involved RBD or impaired olfaction, or both).

In summary, a majority of studies have investigated the value of NM-MRI and the N1 sign in PD and in related movement disorders. In brief, NM-MRI could potentially provide useful disease state biomarkers for clinical trials in the preclinical and prodromal stages and also be used to monitor the progression beginning in early-stage (recently diagnosed or minimally symptomatic) PD.<sup>96</sup> However, biomarkers derived from NM-MRI alone do not seem to be able to reliably distinguish PD from the atypical Parkinsonian disorders, nor will it be sufficient to monitor the progression in patients with moderate to late-stage PD. The reliability and

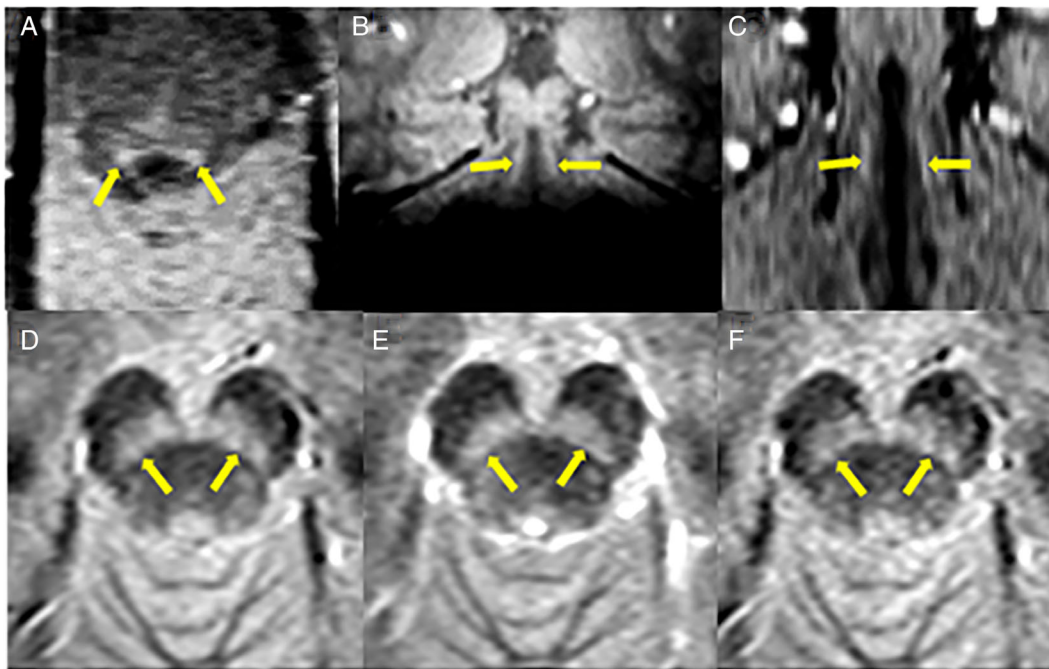


**FIGURE 7:** Visualizing the NM without an MTC pulse. Top row, NM in the LC: (a) From the 6° STAGE data, the spin-density-weighted short TE (7.5 msec) is good enough to visualize the NM because the surrounding CSF is sufficiently suppressed and the high water content of the LC makes it visible. (b) Coronal reformat of the data showing the LC. Both (a) and (b) are from a resolution of 0.67 mm × 1 mm (interpolated to 0.67 mm × 0.67 mm) × 1.34 mm. (c) High-resolution MTC coronal view with a resolution of 0.67 mm × 0.67 mm. Bottom row, NM in the SN: (d) an average over two 3 minutes scans with a 3° flip angle; (e) the usual MTC NM images as a reference (5 minutes scan); and (f) the original 3° flip angle (3 minutes scan). The resolution for figures (d–f) is the same as the resolution in figures (a,b).

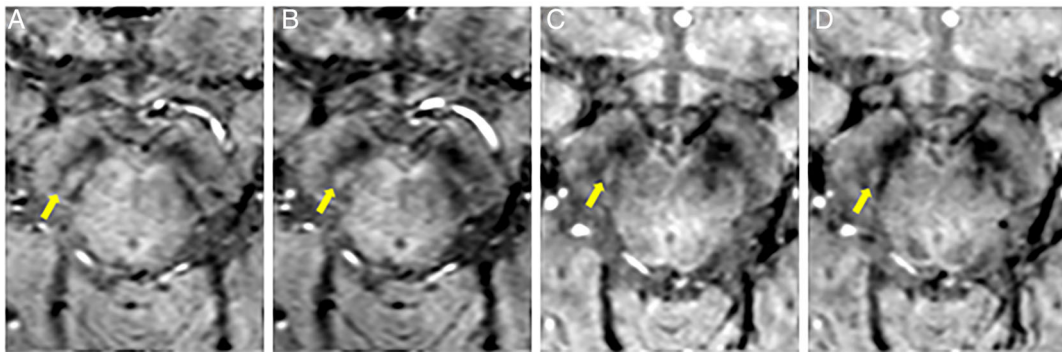


**FIGURE 8: Rapid long-echo imaging using waveSWI.** (a) tSWI of the original third echo (22.5 msec) data, (b) the original third echo magnitude data, (c) the average of the waveSWI 15 msec and 30 msec echoes, and (d) tSWI of this averaged image. The conventional acquisition with  $0.67 \text{ mm} \times 1 \text{ mm} \times 1.34 \text{ mm}$  takes 4.5 minutes per scan (with  $\text{TR} = 29 \text{ msec}$ ) while the waveSWI (even with its longer repeat time of 45 msec) takes only 3 minutes for whole brain coverage. The long echo times help to visualize the N1 sign.

consistency of the NM-related biomarkers need to be further investigated in multisite studies in the future.

### Conclusions and Future Directions

There is considerable ongoing effort in the MR field to find useful imaging biomarkers for PD and related neurodegenerative disorders. It has been found that either using NM volumes and/or the N1 sign (which also is clearly related to the presence of NM) a high sensitivity and specificity can be found for differentiating PD patients from HCs. However, to differentiate between the various Parkinsonian movement disorders will likely require the inclusion of iron measures throughout the DGM. In order to provide definitive assessment of novel biomarkers, hundreds if not thousands of cases should be studied across sites. This is only possible if some level of technical standardization can be reached. One such approach of standardizing the measure NM and iron is STAGE (strategically acquired gradient echo) imaging.<sup>97,98</sup> With this technique, it has been possible to show reproducibility across sites and across manufacturers for the measures of NM and iron content.<sup>14</sup> Once this type of standardized imaging approach has become adopted, this will create a big data environment, which will benefit from the use of AI in comprehensively evaluating the data. Machine learning and radiomics may be the way of the future in investigating a broad variety of features to differentiate PD from other forms of neurodegeneration.<sup>7</sup> Finally, new technical developments in imaging NM and iron simultaneously are promising. New methods such as spin density-weighted 3D gradient echo imaging<sup>14</sup> that do not require an MTC pulse and rely on the increased water content of the NM (Fig. 7) or faster imaging methods such as wave SWI<sup>99</sup> to image the N1 sign with longer echo times (Fig. 8) open the door to more practical imaging of movement disorder patients where motion can be a problem. With a concerted, collaborative effort, the radiology and neurology research communities have the opportunity

to incorporate these methods in large collaborative studies to begin to address these issues, which are significantly important for the care of patients.

### Acknowledgments

The authors thank Peng Liu, Youmin Zhang, and Qiuyun Xu for creating some of the pictures and tables. The authors thank Junchen Li for helping create the nigrosome schematic. The authors thank Mojtaba Jokar for reviewing the manuscript.

### References

1. Fearnley JM, Lees AJ. Ageing and Parkinson's disease: Substantia nigra regional selectivity. *Brain* 1991;114(Pt 5):2283-2301.
2. Damier P, Hirsch E, Agid Y, Graybiel A. The substantia nigra of the human brain: II. Patterns of loss of dopamine-containing neurons in Parkinson's disease. *Brain* 1999;122(8):1437-1448.
3. Wypijewska A, Galazka-Friedman J, Bauminger ER, et al. Iron and reactive oxygen species activity in parkinsonian substantia nigra. *Parkinsonism Relat Disord* 2010;16(5):329-333.
4. He N, Ghassaban K, Huang P, et al. Imaging iron and neuromelanin simultaneously using a single 3D gradient echo magnetization transfer sequence: Combining neuromelanin, iron and the nigrosome-1 sign as complementary imaging biomarkers in early stage Parkinson's disease. *Neuroimage* 2021;230:117810.
5. Takahashi H, Watanabe Y, Tanaka H, et al. Comprehensive MRI quantification of the substantia nigra pars compacta in Parkinson's disease. *Eur J Radiol* 2018;109:48-56.
6. Matsuura K, Maeda M, Tabei KI, et al. A longitudinal study of neuromelanin-sensitive magnetic resonance imaging in Parkinson's disease. *Neurosci Lett* 2016;633:112-117.
7. Cheng Z, He N, Huang P, et al. Imaging the Nigrosome 1 in the substantia nigra using susceptibility weighted imaging and quantitative susceptibility mapping: An application to Parkinson's disease. *NeuroImage Clinical* 2020;25:102103.
8. Langley J, He N, Huddleston DE, et al. Reproducible detection of nigral iron deposition in 2 Parkinson's disease cohorts. *Mov Disord* 2019;34(3):416-419.
9. Langley J, Huddleston DE, Sedlacik J, Boelmans K, Hu XP. Parkinson's disease-related increase of T2\*-weighted hypointensity in substantia nigra pars compacta. *Mov Disord* 2017;32(3):441-449.

10. Biondetti E, Santin MD, Valabregue R, et al. The spatiotemporal changes in dopamine, neuromelanin and iron characterizing Parkinson's disease. *Brain* 2021;144(10):3114-3125.
11. Takahashi H, Watanabe Y, Tanaka H, et al. Quantifying changes in nigrosomes using quantitative susceptibility mapping and neuromelanin imaging for the diagnosis of early-stage Parkinson's disease. *Br J Radiol* 2018;91(1086):20180037.
12. Zarow C, Lyness SA, Mortimer JA, Chui HC. Neuronal loss is greater in the locus coeruleus than nucleus basalis and substantia nigra in Alzheimer and Parkinson diseases. *Arch Neurol* 2003;60(3):337-341.
13. Liu Y, Li J, He N, et al. Optimizing neuromelanin contrast in the substantia nigra and locus coeruleus using a magnetization transfer contrast prepared 3D gradient recalled echo sequence. *Neuroimage* 2020;218:116935.
14. He N, Wu B, Liu Y, et al. STAGE as a multicenter, multivendor protocol for imaging Parkinson's disease: A validation study on healthy controls. *Chin J Acad Radiol* 2022;5(1):47-60.
15. Marsden CD. Neuromelanin and Parkinson's disease. *J Neural Transm Suppl* 1983;19:121-141.
16. Mann DM, Yates PO. Lipoprotein pigments--their relationship to ageing in the human nervous system. II. The melanin content of pigmented nerve cells. *Brain* 1974;97(3):489-498.
17. Purkinje RFJE. Contributions to study of anatomy and physiology of movement disorders. *Mov Disord* 31(suppl 2):2016.
18. Mann DM, Yates PO. Possible role of neuromelanin in the pathogenesis of Parkinson's disease. *Mech Ageing Dev* 1983;21(2):193-203.
19. Gibb WR, Lees AJ. Anatomy, pigmentation, ventral and dorsal subpopulations of the substantia nigra, and differential cell death in Parkinson's disease. *J Neurol Neurosurg Psychiatry* 1991;54(5):388-396.
20. Zucca FA, Bellei C, Giannelli S, et al. Neuromelanin and iron in human locus coeruleus and substantia nigra during aging: Consequences for neuronal vulnerability. *J Neural Transm (Vienna)* 2006;113(6):757-767.
21. Zheng W, Nichol H, Liu S, Cheng YC, Haacke EM. Measuring iron in the brain using quantitative susceptibility mapping and X-ray fluorescence imaging. *Neuroimage* 2013;78:68-74.
22. Zecca L, Gallorini M, Schunemann V, et al. Iron, neuromelanin and ferritin content in the substantia nigra of normal subjects at different ages: Consequences for iron storage and neurodegenerative processes. *J Neurochem* 2001;76(6):1766-1773.
23. Reimao S, Pita Lobo P, Neutel D, et al. Substantia nigra neuromelanin magnetic resonance imaging in de novo Parkinson's disease patients. *Eur J Neurol* 2015;22(3):540-546.
24. Damier P, Hirsch EC, Agid Y, Graybiel AM. The substantia nigra of the human brain. I. Nigrosomes and the nigral matrix, a compartmental organization based on calbindin D(28K) immunohistochemistry. *Brain* 1999;122(Pt 8):1421-1436.
25. Jin Z, Wang Y, Jökar M, et al. Automatic detection of neuromelanin and iron in the midbrain nuclei using a magnetic resonance imaging-based brain template. *Hum Brain Mapp* 2022;43(6):2011-2025.
26. Blazejewski AI, Schwarz ST, Pitiot A, et al. Visualization of nigrosome 1 and its loss in PD: Pathoanatomical correlation and in vivo 7 T MRI. *Neurology* 2013;81(6):534-540.
27. Liu KY, Acosta-Cabrero J, Cardenas-Blanco A, et al. In vivo visualization of age-related differences in the locus coeruleus. *Neurobiol Aging* 2019;74:101-111.
28. Massey LA, Miranda MA, Al-Hellli O, et al. 9.4 T MR microscopy of the substantia nigra with pathological validation in controls and disease. *Neuroimage Clin* 2017;13:154-163.
29. Liu S, Mok K, Neelavalli J, et al. Improved MR venography using quantitative susceptibility-weighted imaging. *J Magn Reson Imaging* 2014;40(3):698-708.
30. Nam Y, Gho SM, Kim DH, Kim EY, Lee J. Imaging of nigrosome 1 in substantia nigra at 3T using multiecho susceptibility map-weighted imaging (SMWI). *J Magn Reson Imaging* 2017;46(2):528-536.
31. Fu KA, Nathan R, Dinov ID, Li J, Toga AW. T2-imaging changes in the nigrosome-1 relate to clinical measures of Parkinson's disease. *Front Neurol* 2016;7:174.
32. Oh SW, Shin NY, Lee JJ, et al. Correlation of 3D FLAIR and dopamine transporter imaging in patients with parkinsonism. *AJR Am J Roentgenol* 2016;207(5):1089-1094.
33. Sung YH, Noh Y, Kim EY. Early-stage Parkinson's disease: Abnormal nigrosome 1 and 2 revealed by a voxelwise analysis of neuromelanin-sensitive MRI. *Hum Brain Mapp* 2021;42(9):2823-2832.
34. Schwarz ST, Mougín O, Xing Y, et al. Parkinson's disease related signal change in the nigrosomes 1-5 and the substantia nigra using T2\* weighted 7T MRI. *Neuroimage Clin* 2018;19:683-689.
35. Langley J, Huddleston DE, Crosson B, Song DD, Factor SA, Hu X. Multimodal assessment of nigrosomal degeneration in Parkinson's disease. *Parkinsonism Relat Disord* 2020;80:102-107.
36. Galgani A, Lombardo F, Della Latta D, et al. Locus Coeruleus magnetic resonance imaging in neurological diseases. *Curr Neurol Neurosci Rep* 2020;21(1):2.
37. Betts MJ, Kirilina E, Otaduy MCG, et al. Locus coeruleus imaging as a biomarker for noradrenergic dysfunction in neurodegenerative diseases. *Brain* 2019;142(9):2558-2571.
38. Fernandes P, Regala J, Correia F, Goncalves-Ferreira AJ. The human locus coeruleus 3-D stereotactic anatomy. *Surg Radiol Anat* 2012;34(10):879-885.
39. Schwarz ST, Xing Y, Tomar P, Bajaj N, Auer DP. In vivo assessment of brainstem depigmentation in Parkinson disease: Potential as a severity marker for multicenter studies. *Radiology* 2017;283(3):789-798.
40. Langley J, Huddleston DE, Liu CJ, Hu X. Reproducibility of locus coeruleus and substantia nigra imaging with neuromelanin sensitive MRI. *Magma (New York, NY)* 2017;30(2):121-125.
41. Watanabe Y, Tanaka H, Tsukabe A, et al. Neuromelanin magnetic resonance imaging reveals increased dopaminergic neuron activity in the substantia nigra of patients with schizophrenia. *PLoS One* 2014;9(8):e104619.
42. Castellanos G, Fernandez-Seara MA, Lorenzo-Betancor O, et al. Automated neuromelanin imaging as a diagnostic biomarker for Parkinson's disease. *Mov Disord* 2015;30(7):945-952.
43. Madelung CF, Meder D, Fuglsang SA, et al. Locus Coeruleus shows a spatial pattern of structural disintegration in Parkinson's disease. *Mov Disord* 2022;37(3):479-489.
44. Doppler CEJ, Kinnerup MB, Brune C, et al. Regional locus coeruleus degeneration is uncoupled from noradrenergic terminal loss in Parkinson's disease. *Brain* 2021;144(9):2732-2744.
45. Zhou C, Guo T, Wu J, et al. Locus Coeruleus degeneration correlated with levodopa resistance in Parkinson's disease: A retrospective analysis. *J Parkinsons Dis* 2021;11(4):1631-1640.
46. Sasaki M, Shibata E, Tohyama K, et al. Neuromelanin magnetic resonance imaging of locus coeruleus and substantia nigra in Parkinson's disease. *Neuroreport* 2006;17(11):1215-1218.
47. Nakane T, Nishihashi T, Kawai H, Naganawa S. Visualization of neuromelanin in the substantia nigra and locus coeruleus at 1.5 T using a 3D-gradient echo sequence with magnetization transfer contrast. *Magn Reson Med* 2008;7(4):205-210.
48. Chen X, Huddleston DE, Langley J, et al. Simultaneous imaging of locus coeruleus and substantia nigra with a quantitative neuromelanin MRI approach. *Magn Reson Imaging* 2014;32(10):1301-1306.
49. Trujillo P, Summers PE, Ferrari E, et al. Contrast mechanisms associated with neuromelanin-MRI. *Magn Reson Med* 2017;78(5):1790-1800.
50. Trujillo P, Summers PE, Smith AK, et al. Pool size ratio of the substantia nigra in Parkinson's disease derived from two different quantitative magnetization transfer approaches. *Neuroradiology* 2017;59(12):1251-1263.
51. Trujillo P, Petersen KJ, Cronin MJ, et al. Quantitative magnetization transfer imaging of the human locus coeruleus. *Neuroimage* 2019;200:191-198.

52. Watanabe T, Tan Z, Wang X, Martinez-Hernandez A, Frahm J. Magnetic resonance imaging of noradrenergic neurons. *Brain Struct Funct* 2019;224(4):1609-1625.
53. Keren NI, Lozar CT, Harris KC, Morgan PS, Eckert MA. In vivo mapping of the human locus coeruleus. *Neuroimage* 2009;47(4):1261-1267.
54. Priovoulos N, Jacobs HI, Ivanov D, Uludağ K, Verhey FR, Poser BA. High-resolution in vivo imaging of human locus coeruleus by magnetization transfer MRI at 3T and 7T. *Neuroimage* 2018;168:427-436.
55. van der Pluijm M, Cassidy C, Zandstra M, et al. Reliability and reproducibility of Neuromelanin-sensitive imaging of the substantia nigra: A comparison of three different sequences. *J Magn Reson Imaging* 2021; 53(3):712-721.
56. Langley J, Huddleston DE, Chen X, Sedlacik J, Zachariah N, Hu X. A multicontrast approach for comprehensive imaging of substantia nigra. *Neuroimage* 2015;112:7-13.
57. Huddleston DE, Langley J, Sedlacik J, Boelmans K, Factor SA, Hu XP. In vivo detection of lateral-ventral tier nigral degeneration in Parkinson's disease. *Hum Brain Mapp* 2017;38(5):2627-2634.
58. Betts MJ, Cardenas-Blanco A, Kanowski M, Jessen F, Düzel E. In vivo MRI assessment of the human locus coeruleus along its rostrocaudal extent in young and older adults. *Neuroimage* 2017;163:150-159.
59. Wengler K, He X, Abi-Dargham A, Horga G. Reproducibility assessment of neuromelanin-sensitive magnetic resonance imaging protocols for region-of-interest and voxelwise analyses. *Neuroimage* 2020;208: 116457.
60. Ye R, O'Callaghan C, Rua C, et al. Locus Coeruleus integrity from 7 T MRI relates to apathy and cognition in parkinsonian disorders. *Mov Disord* 2022;37:1663-1672.
61. Rua C, O'Callaghan C, Ye R, et al. Substantia nigra ferric overload and neuromelanin loss in Parkinson's disease measured with 7T MRI. *medRxiv* 2021. doi:10.1101/2021.04.13.21255416
62. Murty VP, Shermohammed M, Smith DV, Carter RM, Huettel SA, Adcock RA. Resting state networks distinguish human ventral tegmental area from substantia nigra. *Neuroimage* 2014;100:580-589.
63. Uchida Y, Kan H, Sakurai K, et al. Magnetic susceptibility associates with dopaminergic deficits and cognition in Parkinson's disease. *Mov Disord* 2020;35(8):1396-1405.
64. Pauli WM, Nili AN, Tyska JM. A high-resolution probabilistic in vivo atlas of human subcortical brain nuclei. *Sci Data* 2018;5:180063.
65. Keuken MC, Bazin PL, Crown L, et al. Quantifying inter-individual anatomical variability in the subcortex using 7 T structural MRI. *Neuroimage* 2014;94:40-46.
66. Safai A, Prasad S, Chougule T, Saini J, Pal PK, Ingathalikar M. Microstructural abnormalities of substantia nigra in Parkinson's disease: A neuromelanin sensitive MRI atlas based study. *Hum Brain Mapp* 2020; 41(5):1323-1333.
67. Keren NI, Taheri S, Vazey EM, et al. Histologic validation of locus coeruleus MRI contrast in post-mortem tissue. *Neuroimage* 2015;113: 235-245.
68. Ogisu K, Kudo K, Sasaki M, et al. 3D neuromelanin-sensitive magnetic resonance imaging with semi-automated volume measurement of the substantia nigra pars compacta for diagnosis of Parkinson's disease. *Neuroradiology* 2013;55(6):719-724.
69. Krupicka R, Marecek S, Mala C, et al. Automatic substantia nigra segmentation in neuromelanin-sensitive MRI by deep neural network in patients with prodromal and manifest synucleinopathy. *Physiol Res* 2019;68(Suppl 4):S453-S458.
70. Le Berre A, Kamagata K, Otsuka Y, et al. Convolutional neural network-based segmentation can help in assessing the substantia nigra in neuromelanin MRI. *Neuroradiology* 2019;61(12):1387-1395.
71. Nakamura Y, Okada N, Kunitatsu A, Kasai K, Koike S. Anatomical templates of the midbrain ventral tegmental area and substantia nigra for Asian populations. *Front Psych* 2018;9:383.
72. Cho SJ, Bae YJ, Kim JM, et al. Diagnostic performance of neuromelanin-sensitive magnetic resonance imaging for patients with Parkinson's disease and factor analysis for its heterogeneity: A systematic review and meta-analysis. *Eur Radiol* 2021;31(3):1268-1280.
73. Pyatigorskaya N, Magnin B, Mongin M, et al. Comparative study of MRI biomarkers in the substantia nigra to discriminate idiopathic Parkinson disease. *AJNR Am J Neuroradiol* 2018;39(8):1460-1467.
74. Biondetti E, Gaurav R, Yahia-Cherif L, et al. Spatiotemporal changes in substantia nigra neuromelanin content in Parkinson's disease. *Brain* 2020;143(9):2757-2770.
75. He N, Ling H, Ding B, et al. Region-specific disturbed iron distribution in early idiopathic Parkinson's disease measured by quantitative susceptibility mapping. *Hum Brain Mapp* 2015;36(11):4407-4420.
76. Prasuhn J, Prasuhn M, Fellbrich A, et al. Association of Locus Coeruleus and substantia nigra pathology with motor functions in patients with Parkinson disease. *Neurology* 2021;97(10):e1007-e1016.
77. Li Y, Wang C, Wang J, et al. Mild cognitive impairment in de novo Parkinson's disease: A neuromelanin MRI study in locus coeruleus. *Mov Disord* 2019;34(6):884-892.
78. Garcia-Lorenzo D, Longo-Dos Santos C, Ewencyk C, et al. The coeruleus/subcoeruleus complex in rapid eye movement sleep behaviour disorders in Parkinson's disease. *Brain* 2013;136(Pt 7):2120-2129.
79. Jacobs HIL, Muller-Ehrenberg L, Priovoulos N, Roebroek A. Curvilinear locus coeruleus functional connectivity trajectories over the adult lifespan: A 7T MRI study. *Neurobiol Aging* 2018;69:167-176.
80. Liu KY, Marijatta F, Hämmerer D, Acosta-Cabrero J, Düzel E, Howard RJ. Magnetic resonance imaging of the human locus coeruleus: A systematic review. *Neurosci Biobehav Rev* 2017;83:325-355.
81. Sulzer D, Cassidy C, Horga G, et al. Neuromelanin detection by magnetic resonance imaging (MRI) and its promise as a biomarker for Parkinson's disease. *NPJ Parkinson's Dis* 2018;4:11.
82. Heim B, Krismer F, De Marzi R, Seppi K. Magnetic resonance imaging for the diagnosis of Parkinson's disease. *J Neural Transm (Vienna)* 2017;124(8):915-964.
83. Langkammer C, Pirpamer L, Seiler S, et al. Quantitative susceptibility mapping in Parkinson's disease. *PLoS One* 2016;11(9):e0162460.
84. Ropele S, Langkammer C. Iron quantification with susceptibility. *NMR Biomed* 2017;30(4):30.
85. Barbagallo G, Sierra-Pena M, Nemmi F, et al. Multimodal MRI assessment of nigro-striatal pathway in multiple system atrophy and Parkinson disease. *Mov Disord* 2016;31(3):325-334.
86. Mazzucchi S, Frosini D, Costagli M, et al. Quantitative susceptibility mapping in atypical Parkinsonisms. *NeuroImage Clin* 2019;24: 101999.
87. Ohtsuka C, Sasaki M, Konno K, et al. Differentiation of early-stage parkinsonisms using neuromelanin-sensitive magnetic resonance imaging. *Parkinsonism Relat Disord* 2014;20(7):755-760.
88. Jin L, Wang J, Wang C, et al. Combined visualization of nigrosome-1 and neuromelanin in the substantia nigra using 3T MRI for the differential diagnosis of essential tremor and de novo Parkinson's disease. *Front Neurol* 2019;10:100.
89. Wang J, Huang Z, Li Y, et al. Neuromelanin-sensitive MRI of the substantia nigra: An imaging biomarker to differentiate essential tremor from tremor-dominant Parkinson's disease. *Parkinsonism Relat Disord* 2019;58:3-8.
90. Kitao S, Matsusue E, Fujii S, et al. Correlation between pathology and neuromelanin MR imaging in Parkinson's disease and dementia with Lewy bodies. *Neuroradiology* 2013;55(8):947-953.
91. Jankovic J, McDermott M, Carter J, et al. Variable expression of Parkinson's disease: A base-line analysis of the DATATOP cohort. The Parkinson Study Group. *Neurology* 1990;40(10):1529-1534.
92. Wang L, Yan Y, Zhang L, Liu Y, Luo R, Chang Y. Substantia nigra neuromelanin magnetic resonance imaging in patients with different subtypes of Parkinson disease. *J Neural Transm (Vienna)* 2021;128(2): 171-179.



93. Xiang Y, Gong T, Wu J, et al. Subtypes evaluation of motor dysfunction in Parkinson's disease using neuromelanin-sensitive magnetic resonance imaging. *Neurosci Lett* 2017;638:145-150.
94. Sommerauer M, Fedorova TD, Hansen AK, et al. Evaluation of the noradrenergic system in Parkinson's disease: An 11C-MeNER PET and neuromelanin MRI study. *Brain* 2018;141(2):496-504.
95. Ehrminger M, Latimier A, Pyatigorskaya N, et al. The coeruleus/subcoeruleus complex in idiopathic rapid eye movement sleep behaviour disorder. *Brain* 2016;139(Pt 4):1180-1188.
96. Mitchell T, Lehericy S, Chiu SY, Strafella AP, Stoessl AJ, Vaillancourt DE. Emerging neuroimaging biomarkers across disease stage in Parkinson disease: A review. *JAMA Neurol* 2021;78(10):1262-1272.
97. Chen Y, Liu S, Wang Y, Kang Y, Haacke EM. STrategically acquired gradient Echo (STAGE) imaging, part I: Creating enhanced T1 contrast and standardized susceptibility weighted imaging and quantitative susceptibility mapping. *Magn Reson Imaging* 2018;46:130-139.
98. Haacke EM, Chen Y, Utriainen D, et al. STrategically acquired gradient Echo (STAGE) imaging, part III: Technical advances and clinical applications of a rapid multi-contrast multi-parametric brain imaging method. *Magn Reson Imaging* 2020;65:15-26.
99. Conklin J, Longo MGF, Cauley SF, et al. Validation of highly accelerated wave-CAIPI SWI compared with conventional SWI and T2\*-weighted gradient recalled-echo for routine clinical brain MRI at 3T. *AJNR Am J Neuroradiol* 2019;40(12):2073-2080.